Interference effects at a dielectric plate applied as a high-power-laser attenuator

Peter Gregorčič,* Aleš Babnik, and Janez Možina

Faculty of Mechanical Engineering, University of Ljubljana, Aškerčeva 6, 1000 Ljubljana, Slovenia
**peter.gregorcic@fs.uni-lj.si*

Abstract: The interference effects caused by the Fresnel reflections of a Gaussian beam on the boundaries of a dielectric plate, which can be considered as a Fabry-Perot etalon, were theoretically and experimentally investigated. In addition to the incident angle and the polarization of the incident light, two additional parameters—the plate's parallelism and the temperature—which are often neglected, were analyzed. Based on the theoretical predictions and the measured behavior of the transmittance of the dielectric plate a new, temperature-controlled variable high-power-laser attenuator is proposed. Unwanted changes in the plate's transmittance caused by the absorption of laser pulses within the plate are also presented. These phenomena are important in many applications where dielectric plates are used for a variety of purposes.

OCIS codes: (260.3160) Interference; (140.0140) Lasers and laser optics; (140.6810) Thermal effects.

References and links

1. R. O. Rice, and J. D. Macomber, "Attenuation of giant laser pulses by absorbing filters," Appl. Opt. **14**(9), 2203–2206 (1975).
2. R. M. A. Azzam, "Tilted parallel dielectric slab as a multilevel attenuator for incident p- or s-polarized light," Appl. Opt. **48**(2), 425–428 (2009).
3. Y. H. Wu, Y. H. Lin, Y. Q. Lu, H. W. Ren, Y. H. Fan, J. R. Wu, and S. T. Wu, "Submillisecond response variable optical attenuator based on sheared polymer network liquid crystal," Opt. Express **12**(25), 6382–6389 (2004).
4. H. Lotem, A. Eyal, and A. R. Shuker, "Variable attenuator for intense unpolarized laser beams," Opt. Lett. **16**(9), 690–692 (1991).
5. D. Gauden, D. Mechin, C. Vaudry, P. Yvernault, and D. Pureur, "Variable optical attenuator based on thermally tuned Mach-Zehnder interferometer within a twin core fiber," Opt. Commun. **231**(1-6), 213–216 (2004).
6. K. Bennett, and R. L. Byer, "Computer-controllable wedged-plate optical-variable attenuator," Appl. Opt. **19**(14), 2408–2412 (1980).
7. J. Staromlynska, R. A. Clay, and K. F. Dexter, "Variable optical attenuator for use in the visible spectrum," Appl. Opt. **26**(18), 3827–3830 (1987).
8. J. H. Lehman, D. Livigni, X. Y. Li, C. L. Cromer, and M. L. Dowell, "Reflective attenuator for high-energy laser measurements," Appl. Opt. **47**(18), 3360–3363 (2008).
9. M. J. Mughal, and N. A. Riza, "Compact acoustooptic high-speed variable attenuator for high-power applications," IEEE Photon. Technol. Lett. **14**(4), 510–512 (2002).
10. H. B. Yu, G. Y. Zhou, C. F. Siong, and L. Feiwen, "A variable optical attenuator based on optofluidic technology," J. Micromech. Microeng. **18**(11), 115016 (2008).
11. J. C. Cotteverte, F. Bretenaker, and A. Lefloch, "Jones matrices of a tilted plate for Gaussian beams," Appl. Opt. **30**(3), 305–311 (1991).
12. H. Kogelnik, and T. Li, "Laser beams and resonators," Appl. Opt. **5**(10), 1550–1567 (1966).
13. S. Nemoto, "Waist shift of a Gaussian-beam by a dielectric plate," Appl. Opt. **28**(9), 1643–1647 (1989).
14. E. Hecht, *Optics* (2nd Edition, Addison Wesley, 1987), pp. 100.
15. H. Abu-Safia, R. Al-Tahtamouni, I. Abu-Aljarayesh, and N. A. Yusuf, "Transmission of a Gaussian-beam through a Fabry-Perot interferometer," Appl. Opt. **33**(18), 3805–3811 (1994).
16. P. Gregorčič, T. Požar, and J. Možina, "Quadrature phase-shift error analysis using a homodyne laser interferometer," Opt. Express **17**(18), 16322–16331 (2009).
17. T. Požar, P. Gregorčič, and J. Možina, "Optical measurements of the laser-inducedultrasonic waves on moving objects," Opt. Express **17**(25), 22906–22911 (2009).
18. P. Gregorčič, R. Petkovšek, J. Možina, and G. Močnik, "Measurements of cavitation bubble dynamics based on a beam-deflection probe," Appl. Phys., A Mater. Sci. Process. **93**(4), 901–905 (2008).

#121165 - $15.00 USD Received 9 Dec 2009; revised 13 Jan 2010; accepted 28 Jan 2010; published 11 Feb 2010

1. Introduction

The power of an optical beam can be reduced by four basic physical phenomena: absorption [1], reflection [2], polarization [3,4] and interference [5]. The ideal laser attenuator should enable a uniform power reduction over a wide dynamic range, should not significantly affect the beam's geometrical (diameter, divergence, intensity profile, direction) and polarization properties [6], and should have a simple, robust, and inexpensive mechanical and optical design [7]. Among the various attenuation designs [1,2,4–10], several principles [1,6,8] can be used for the attenuation of high-peak-power laser beams, where the main obstacles arise from damage and heating instabilities [1].

One example of a commercially available high-power-laser attenuator is based on the Fresnel transmissions through two pairs of wedged plates [6]. Here, the attenuation is achieved by Fresnel reflections on the surfaces of the plates rather than by absorption in the plates. Since no coating is involved, such an attenuator enables high-power handling and can be used for a broad range of wavelengths. To avoid the complex tilting mechanism of four wedge plates an uncoated dielectric plate can be implemented as a simple high-power-laser attenuator based on multiple reflections. In this case, the variation of the attenuation can be achieved through the tilt of a single window or by changing the number of plates being utilized. However, to use a tilted parallel dielectric plate as a multilevel attenuator, the temperature, the small wedge angle, and other effects need to be investigated [2].

This paper investigates the interference effects caused by the reflections on the boundaries of a dielectric plate. A great deal of the interest in these effects arises from the many applications where dielectric plates are involved for a variety of purposes: from Brewster windows and etalons for mode selection [11] to multilevel, high-power-laser attenuators [2]. We describe these effects in terms of the multiple reflections of a Gaussian beam within a thin plate. Here, the interference takes place among the successively reflected and transmitted beams. When the plate is thin in comparison with the beam-waist radius, the intensity profile of the transmitted beam and its direction are not significantly altered.

We measured the angle and the temperature dependence of a thin dielectric plate's transmittance and compare them with theoretical results. The dependence of interference phenomena with respect to the beam's incident angle results in transmittance oscillations, and this was studied by Cotteverte et al. [11]. However, they considered only the first two transmitted beams, which led to the wrong results at large angles. Their inappropriate physical assumption led to a misinterpretation of the results for a thin plate when they assigned the decrease of the interference maxima with the angle to the limited geometry of the Gaussian beam. In our analysis sufficient transmitted beams are taken into account, so the error arising from the remaining beams is less than 1% at all angles. We show experimentally that the main contribution to the decrease of the interference maxima—when the plate is thin in comparison with the beam-waist radius—results from the small wedge, i.e., the degree of the plate's parallelism.

The main goal of our paper is a presentation of the temperature-dependent interference phenomena that can be utilized for a manipulation of the plate's attenuation or can be considered as unwanted effects. In this paper both aspects are covered. The application of a variable laser attenuator based on a thin dielectric plate and temperature regulation is demonstrated as a utilization of the temperature-dependent interference effects. Here, the absorption of the laser energy in the plate should be as low as possible to avoid damages and other unwanted effects, and its transmittance is changed by the interference due to the different thicknesses and refractive indices for the different temperatures of the plate. On the other hand, when the absorption of the laser energy is significant, unwanted effects need to be taken into account. To provide a qualitative demonstration of this, we present measurements of the plate's transmittance during its absorption of high-power-laser pulses. In this case, the plate's transmission changes with the pulses due to the heating caused by the absorption of energy from the high-power laser.

#121165 - $15.00 USD Received 9 Dec 2009; revised 13 Jan 2010; accepted 28 Jan 2010; published 11 Feb 2010

2. Theory

The electric field reflectance r and transmission t for a single dielectric boundary depend on the angle of incidence θ_i, the polarization of the light and the ratio n between the refractive indices of the incident and the transmitting media. For an uncoated plate and an arbitrary polarization they can be conveniently described using the Jones matrices:

$$r(\theta_i)=\begin{bmatrix} r_s(\theta_i) & 0 \\ 0 & r_p(\theta_i) \end{bmatrix}, \quad t(\theta_i)=\begin{bmatrix} t_s(\theta_i) & 0 \\ 0 & t_p(\theta_i) \end{bmatrix}.$$

Here, the subscripts s and p stand for the linear polarizations perpendicular (s-polarization) and parallel (p-polarization) to the plane of incidence, respectively. The electric field transmission ($t_{s,p}$) and reflectance ($r_{s,p}$) are given by the Fresnel laws.

If E_s and E_p are the electric field components for both polarizations, the Jones vector **E** for the polarized light and the reflected intensity I_r are defined as:

$$\mathbf{E}=\begin{bmatrix} E_s \\ E_p \end{bmatrix}, \quad I_r \propto \left(r\cdot\mathbf{E}\right)^{\dagger}\cdot\left(r\cdot\mathbf{E}\right)=E_s^2R_s(\theta_i)+E_p^2R_p(\theta_i),$$

where $R_{s,p}\left(\theta_i\right)=r_{s,p}^{*}r_{s,p}$ represents the intensity (or power) reflectivity for both polarizations and the dagger denotes the conjugate transpose. The intensity reflectivity $R(\theta_i)$ for an arbitrary polarization is defined as the ratio of the reflected and the incident intensities and can be written as:

$$\begin{gathered} R(\theta_i)=\frac{I_s}{I}R_s(\theta_i)+\frac{I_p}{I}R_p(\theta_i), \\ R_s=\left(\frac{\sin(\theta_t-\theta_i)}{\sin(\theta_t+\theta_i)}\right)^2, \quad R_p=\left(\frac{\tan(\theta_t-\theta_i)}{\tan(\theta_t+\theta_i)}\right)^2, \end{gathered} \tag{1}$$

where I stands for the incident intensity, and the angle of refraction θ_t can be calculated using Snell's law. The intensities for both polarizations are denoted by I_s and I_p, respectively. For unpolarized light, the ratios I_s/I and I_p/I are equal to 1/2.

A dielectric plate made using a material with the refractive index n and thickness d can be considered as a Fabry-Perot etalon (FPE) having two reflecting surfaces that have the reflectivity $R(\theta_i)$ and are separated by a distance d. When a monochromatic laser light is incident upon the dielectric plate, multiple reflections take place inside the plate, leading to successive reflected and transmitted beams. If the laser beam can be described as the fundamental mode of a coherent Gaussian beam (TEM_{00} mode) and the absorption within the plate is neglected, the power transmittance of the interference attenuator can be calculated using the Jones matrices [11] as follows.

The fundamental mode of the Gaussian beam is given by [12]:

$$\begin{gathered} \mathbf{E}(x,y,z)=\begin{bmatrix} E_{0s} \\ E_{0p} \end{bmatrix}\frac{w_0}{w(z)}\exp\left(-\frac{x^2+y^2}{w^2(z)}\right)\exp\left(-ik\frac{x^2+y^2}{2\rho(z)}\right)\exp\left(-i\left[kz-\eta(z)\right]\right), \\ w^2(z)=w_0^2\left[1+\frac{z^2}{z_0^2}\right], \quad z_0=\frac{\pi w_0^2}{\lambda}, \quad \rho(z)=z+\frac{z_0^2}{z}, \quad k=\frac{2\pi}{\lambda}, \quad \eta(z)=\arctan\left(\frac{z}{z_0}\right). \end{gathered} \tag{2}$$

Here, $\mathbf{E_0}$ stands for the amplitude of the electric field at the center of the beam waist, k is the wave number in the z-direction, λ is the wavelength in the vacuum, w_0 is the beam-waist radius, z_0 is the Rayleigh length, while $w(z)$, $\rho(z)$ and $\eta(z)$ are: the beam half-width; the radius of the wave front curvature; and a phase-shift difference between the Gaussian beam and the ideal plane wave at the distance z from the waist, respectively. The beam half-width, called

#121165 - $15.00 USD Received 9 Dec 2009; revised 13 Jan 2010; accepted 28 Jan 2010; published 11 Feb 2010

also a spot size, corresponds to the distance from the beam's center, where the field's amplitude decays to 1/*e* of its maximum.

Figure 1(a) shows a Gaussian beam that is incident upon a dielectric plate, making an angle θ_i with the surface normal. From the geometry presented in Fig. 1(a) it can be seen that the transverse displacement Δx between the two adjacent, reflected beams appears in addition to the path difference between the successive transmitted beams. The electric field of the *m*-th transmitted beam can be given by:

$$\mathbf{E}_m = \mathbf{A}\frac{w_0}{w(z_m)}\exp\left(-\frac{\left[x-m\Delta x\right]^2+y^2}{w^2(z_m)}-ik\frac{\left[x-m\Delta x\right]^2+y^2}{2\rho(z_m)}\right)\exp\left(-i\left[\delta_0+m\delta-\eta(z_m)\right]\right),$$

$$\mathbf{A}=\begin{bmatrix} t_s{}^2 r_s{}^{2m} E_{0s} \\ t_p{}^2 r_p{}^{2m} E_{0p} \end{bmatrix}, \quad \Delta x = 2d\tan\theta_t\cos\theta_i, \quad \delta = 2kdn\cos\theta_t + 2\delta_r,$$

$$z_m = D+\frac{d}{n\cos\theta_t}\left(1-n\cos\left[\theta_i-\theta_t\right]\right)+\frac{2md}{n\cos\theta_t}\left(1-n\sin\theta_t\sin\theta_i\right), \tag{3}$$

where the transmitted beam parameters (w, ρ and η) depend on the traveled distance z_m, which is a function of the distance D between the laser-beam source and the measured surface, the thickness of the plate d, its refractive index n and the angle of the incidence θ_i. Here, the propagation through the dielectric medium with the refractive index n [13] should be taken into account. The phase shift of the first transmitted beam and the phase-shift difference for one round trip in the plate are denoted by δ_0 and δ, respectively. The vector **A** contains the polarization as well as the reflectance and transmittance for the *m*-th transmitted field.

The reflection of the beam at the dielectric boundary changes the amplitude and the phase of the reflected electric field. The amplitude of the reflected beam is described by the real coefficients $r_{s,p}$, while the δ_r in Eq. (3) stands for the phase change. For the purpose of our calculations, only the internal reflections need to be taken into consideration. The phase change δ_r is defined as [14]:

$$\delta_r = \begin{cases} 0 \ ; \text{(p-polarization)} \\ \pi \ ; \ \theta_t < \theta_B \ \text{(s-polarization)}, \\ 0 \ ; \ \theta_t > \theta_B \ \text{(s-polarization)} \end{cases} \tag{4}$$

where θ_B stands for the Brewster angle. The expressions for the angles above the critical angle are omitted from Eq. (4), since the angle of refraction θ_t never exceeds the critical angle. According to Eq. (4), the term $2\delta_r$ in Eq. (3) is either 0 or 2π and therefore does not change the electric field of the *m*-th transmitted beam.

The transmitted electric field $\mathbf{E}_t$ and the corresponding intensity I_t at any point can be expressed as the sum of the successive output beams:

$$\mathbf{E}_t(x,y,z) = \sum_{m=0}^{\infty} E_m(x_m,y,z_m), \qquad I_t(x,y,z) \propto \sum_{l=0}^{\infty}\sum_{m=0}^{\infty} \mathbf{E}_l^{\dagger}(x_l,y,z_l)\mathbf{E}_m(x_m,y,z_m). \tag{5}$$

Since the power-transmission coefficient of the plate is equal to the ratio between the input and the output powers, the intensity in Eq. (5) should be integrated over the diffracting aperture. In the case when the plate is thin, the beam parameters (w, ρ and η) are approximately constant and the transmitted power P_t can be calculated from the transmitted intensity as:

#121165 - $15.00 USD Received 9 Dec 2009; revised 13 Jan 2010; accepted 28 Jan 2010; published 11 Feb 2010

$$P_t = I_0 \frac{w_0^2}{w^2}\left(1-R(\theta_i)\right)^2 \sum_{l=0}^{\infty}\sum_{m=0}^{\infty} R(\theta_i)^{m+l} \int_{-\infty}^{\infty} \exp\left(-\frac{2y^2}{w^2}\right)dy$$
$$\times \int_{-\infty}^{\infty} \exp\left(-\frac{(x-m\Delta x)^2+(x-l\Delta x)^2}{w^2}\right)\cos\left(k\frac{(x-l\Delta x)^2-(x-m\Delta x)^2}{2\rho}+(l-m)\delta\right)dx. \quad (6)$$

The cosine in Eq. (6) can be divided into the product of sines and cosines using trigonometric relations. Since the integral of the product of an exponential and sine function is zero, and the following identity is valid:

$$\int_{-\infty}^{\infty} \exp\left(-ax^2\right)\cos\left(bx\right)dx = \sqrt{\frac{\pi}{a}}\exp\left(-\frac{b^2}{4a}\right),$$

the power-transmission coefficient for a Gaussian beam $T_P^{(G)}$ can be expressed as:

$$T_P^{(G)} = \left(1-R(\theta_i)\right)^2 \sum_{l=0}^{\infty}\sum_{m=0}^{\infty} R(\theta_i)^{m+l} \exp\left\{-\frac{\Delta x^2 (m-l)^2}{2}\left(\frac{k^2w^2}{4\rho^2}+\frac{1}{w^2}\right)\right\}\cos\left((m-l)\delta\right). \quad (7)$$

Here, the power reflectance $R(\theta_i)$, defined by Eq. (1), is a function of the incident angle and depends on the polarization of the incident light. Using the relations defined by Eq. (2), the term in the curly brackets in Eq. (7) reduces to $-\frac{\Delta x^2}{2w_0^2}(m-l)^2$. Therefore, the power-transmission coefficient for a Gaussian beam can be described as:

$$T_P^{(G)} = \left(1-R(\theta_i)\right)^2 \sum_{l=0}^{\infty}\sum_{m=0}^{\infty} R(\theta_i)^{m+l} \exp\left\{-\frac{\Delta x^2}{2w_0^2}(m-l)^2\right\}\cos\left((m-l)\delta\right). \quad (8)$$

In the limit of the plane wave ($w_0 \to \infty$), the term in the curly brackets in Eq. (8) goes to zero and the power-transmission coefficient for the dielectric plate yields the well-known Airy function [15]:

$$T_P^{(PW)} = \frac{1}{1+\frac{4R(\theta_i)}{\left(1-R(\theta_i)\right)^2}\sin^2\left(\delta/2\right)}, \quad (9)$$

where $T_P^{(PW)}$ stands for the power-transmission coefficient for a plane wave and the phase-shift difference δ between each succeeding reflection is given in Eq. (3).

In the case of the Gaussian beam, the exponential term in Eq. (8) is equal to 1 only for $m = l$ or $\Delta x = 0$, i.e., for normal incidence. In all other cases it is smaller than 1 and therefore reduces the amplitude of the fringes corresponding to the plane wave. This phenomenon can be explained by the overlapping between the reflected beams. Since the Gaussian beam is limited, the overlapping between neighboring beams (i.e., $m \neq l$) at large angles is reduced. From the term in the curly brackets in Eq. (8) it can be concluded that the limited beam effects depend on the ratio between the transverse displacement Δx and the beam-waist radius w_0, and does not depend on the distance between the beam source and the plate's position.

3. Experimental setup

For the measurements of the interference phenomena caused by multiple reflections on the boundaries of a dielectric plate we put together the experimental setup shown in Figs. 1(b) and 1(c). As a dielectric plate we applied a 140-μm-thick polished borosilicate glass plate with a refractive index $n = 1.52$ and a calculated thermal diffusivity $D = \kappa/(\rho c_p) = 4.8\times10^{-7}$ m^2 s^{-1}. Here, $\kappa = 0.96$ W m^{-1} K^{-1} stands for the thermal conductivity, $\rho = 2510$ kg m^{-3} is the density,

#121165 - $15.00 USD Received 9 Dec 2009; revised 13 Jan 2010; accepted 28 Jan 2010; published 11 Feb 2010

and c_p = 800 J kg^{-1} K^{-1} is the specific heat capacity. The flatness of the plate was λ/10 at 633 nm. We tested three plates with equal thickness and flatness, but different parallelism. The parallelism was measured by a homodyne quadrature laser interferometer [16] and was 200 μrad, 45 μrad, and 15 μrad for the individual plates.

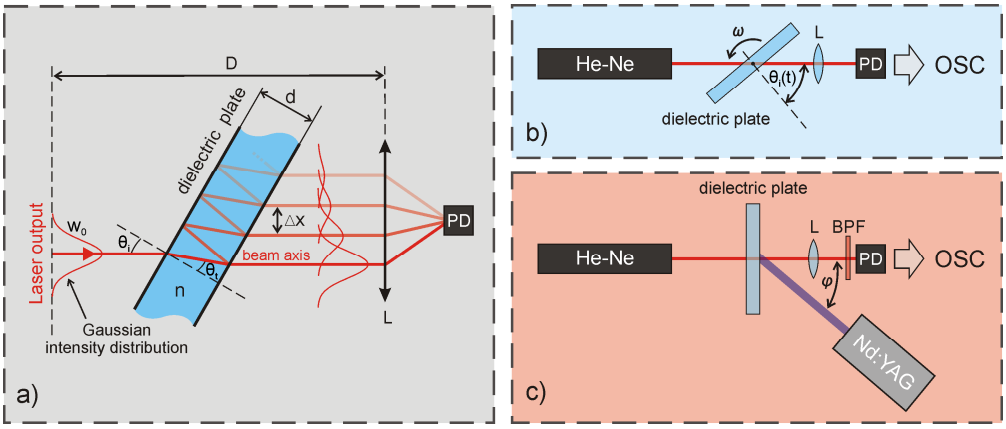

Fig. 1. a) The propagation of a Gaussian beam through the dielectric plate of thickness d and refractive index n. The probe-beam-waist radius is denoted by w_0, D is the distance between the laser output and the lens L, which collects the transmitted light into the photodiode PD. When the beam incidences the dielectric plate with an angle θ_i, the transverse displacement Δx between two adjacent reflected beams needs to be taken into account. b) The experimental setup for measurements of the angle and the temperature-dependent interference effects. A He-Ne laser was used as the probe beam. The dielectric plate was rotated with a constant angular velocity ω. c) Measurements of the plate's transmittance during the absorption of high-power-laser pulses. A fourth-harmonic-generation Nd-YAG laser (λ = 266 nm) was used as an excitation laser. A band-pass filter BPF for the probe beam was placed in front of the PD.

Transmission measurements were performed with the He-Ne laser probe beam (λ = 633 nm) using the beam-waist radius w_0 = 400 μm. The spot size on the plate was w = 448 μm and the radius of curvature was ρ = 1.98 m. The cylindrical head of the polarized He-Ne laser was rotated so that the linear polarization of the probe beam was perpendicular to the plane of incidence (s-polarization). The absorption of a He-Ne light within the thin plate can be neglected, since the absorption coefficient μ was estimated to be less than 0.7 m^{-1}.

In the first set of measurements related to the angle-dependent interference effects (see Fig. 1(b)) the dielectric plate, maintained at a constant room temperature, was rotated around the vertical axes with a constant angular velocity ω = 31.4 s^{-1}. In this way the transmission of the plate was measured as a function of the incident angle θ_i. The transmitted light was collected by a lens (L) and measured by a photodiode (PD) located at the focus of the lens.

When the temperature-dependent effects were investigated, the transmission of the rotated plate was measured at different temperatures of the plate. The temperature was shifted from 325 K to 545 K with steps of ~5 K. During a single measurement, i.e., a measurement over all the incident angles, the temperature of the plate was constant and uniform.

The second part of our experimental investigation was a qualitative study of the interference effects due to heating of the plate, caused by the absorption of high-power-laser pulses (see Fig. 1(c)). For this purpose we employed a fourth-harmonic-generation Nd-YAG laser (λ = 266 nm) as a heating source (the excitation laser) due to its high absorption coefficient in borosilicate glass. The absorption coefficient was evaluated by UV-vis spectrophotometer (Hewlett Packard 8453) to be higher than 7 × 10^4 m^{-1}. The duration of the excitation laser pulse was 5 ns, the repetition rate was 20 Hz, the beam radius was 1.5 mm, and the pulse energy was 13 mJ. A fraction of the excitation-laser energy (0.5 mJ per pulse) was reflected from the front surface of the plate, while the rest (12.5 mJ per pulse) was absorbed within the plate.

#121165 - $15.00 USD Received 9 Dec 2009; revised 13 Jan 2010; accepted 28 Jan 2010; published 11 Feb 2010

The dielectric plate was fixed perpendicular to the He-Ne probe beam during this set of measurements, while the excitation beam was placed at an angle φ of 25 degrees with respect to the plate's normal. Both beams were crossed concentrically on the plate. A band-pass filter (BPF) was placed in front of the photodiode to eliminate the light from the excitation laser.

A single measurement was performed in a time period of 40 s. In the first 25 s a total of 500 pulses were absorbed in the plate, increasing its temperature from room temperature (300 K) to 490 K, where steady-state conditions were achieved. After that the excitation laser was switched off and the transmittance was measured during the plate's cooling.

4. Results and discussion

Figure 2 shows the transmittance of the 140-μm-thick dielectric plate (n = 1.52) as a function of the incident angle. It should be noted that the transmittance in our case reflects the spatially averaged transmitted power and does not consider the spatial distortion of the transmitted beam profile. Both the theoretical and experimental results revealed the typical behavior of multiple-reflected interference phenomena, which manifests itself in transmittance oscillations.

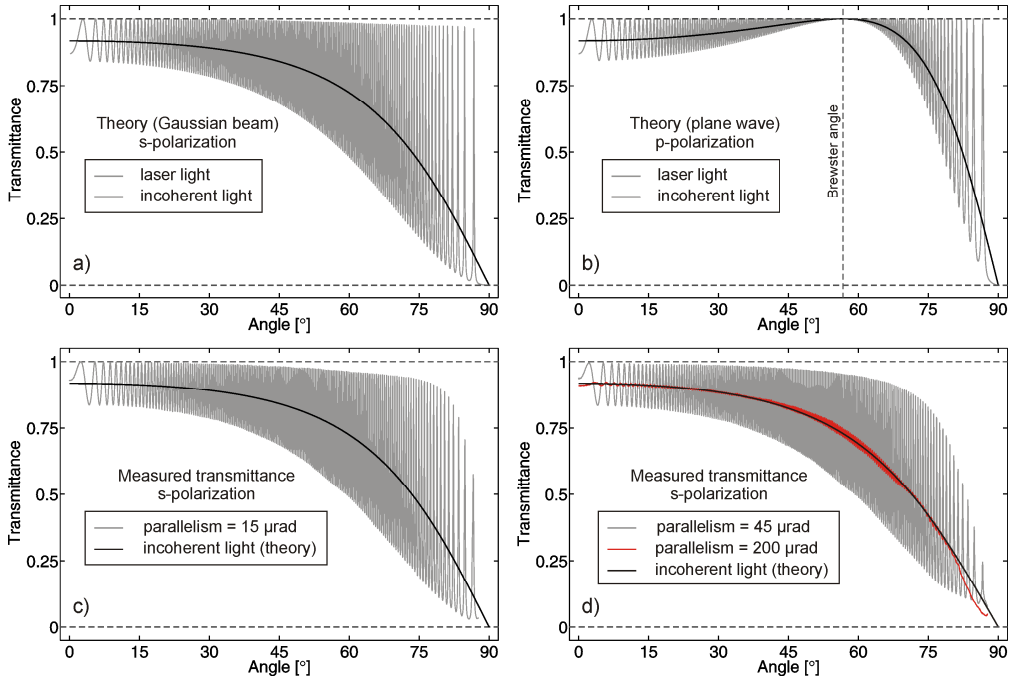

Fig. 2. The transmittance of a dielectric plate as a function of the incident angle. The black curve shows the theoretical results (Eq. (10)) for incoherent light. a) Theoretical transmittance of the plan-parallel plate for an s-polarized Gaussian beam. b) Theoretical transmittance of the plan-parallel plate for the p-polarized plane wave. c) The measured transmittance for the s-polarized probe beam. The parallelism of the plate was 15 μrad. d) The measured transmittance of the plates with different parallelisms for the s-polarized probe beam. The plate's parallelisms were 45 μrad (the gray curve) and 200 μrad (the red curve).

Theoretical results (Figs. 2(a) and 2(b)) were determined for both polarizations in order to show the influence of the polarization of the incident light. In the case of the p-polarized light (Fig. 2(b)), the incident light is perfectly transmitted through the plate, with no reflections, when the incident angle is equal to the Brewster angle θ_B. Therefore, at that angle, defined as $\tan(\theta_B) = n$, the transmittance oscillations disappear.

Theoretical results were also obtained with both theories—for the Gaussian beam (Eq. (8), see Fig. 2 (a)) and for the plane wave (Eq. (9), see Fig. 2 (b)). In the case of the Gaussian

#121165 - $15.00 USD Received 9 Dec 2009; revised 13 Jan 2010; accepted 28 Jan 2010; published 11 Feb 2010

beam (Fig. 2(a)), the beam parameters used in our calculations are equal to the characteristics of our probe beam described in the Experimental setup. Equation (8) includes an infinite series of transmitted beams. However, the first 25 transmitted beams were taken into account during our calculation. This result was compared with the transmittance calculated from the first 50 transmitted beams. The difference between both results was less than 1% at all the incident angles. On the other hand, when only the first two transmitted beams are considered, as in Ref [11], this error increases with the incident angle, from 10% for the transmittance peak at 65° to 86% for the last peak at 87°.

A comparison between the transmittance of a Gaussian beam (Fig. 2(a)) and the plane wave (Fig. 2(b)) through a dielectric plate shows the following. In the case of the plane wave, which is not spatially limited, the peak values of the transmittance oscillations are equal to 1 for all the incident angles. On the other hand, the Gaussian beam is spatially limited and therefore the peak values of the oscillations diminish at large angles. This happens because the successively reflected and transmitted beams are only partially overlapped. The described effect is small when the beam-waist radius w_0 is large in comparison with the plate's thickness d.

If the incident light is incoherent, the transmittance oscillations disappear and the transmittance of a dielectric plate can be expressed as:

$$T_P^{(NC)} = (1-R)^2 \sum_{l=0}^{\infty} R^{2l} = \frac{(1-R(\theta_i))^2}{1-R(\theta_i)^2}, \tag{10}$$

where $R(\theta_i)$ is the power reflectivity defined by Eq. (1). The results of Eq. (10) are shown in Fig. 2 with the solid, black curve.

The measured transmittance of the 140-μm-thick dielectric plate (n = 1.52) as a function of the incident angle is presented in Figs. 2(c) and 2(d). Figure 2(c) shows the transmittance for the plate with a parallelism of 15 μrad. A comparison of these results with the corresponding theoretical results in Fig. 2(a) reveals a good agreement between the experiment and the theory. However, in contrast to the theoretical predictions, the experimental results show a larger decrease in the interference maxima at large angles. This happens because the dielectric plate is not perfectly parallel; instead, it forms a small wedge. The wedge changes the plate's thickness, so particular points of the probe-beam profile experience a different transmittance. To prove this we measured the transmittance of plates with equal thickness and flatness, but different parallelisms. The gray and the red curves in Fig. 2(d) show the measured transmittance for the plates with parallelisms of 45 μrad and 200 μrad, respectively. It is clear that the interference maxima decrease when the wedge increases from 15 μrad (the gray curve in Fig. 2 (c)) to 45 μrad (the gray curve in Fig. 2(d)). In the case of the plate with a parallelism of 200 μrad, i.e., the 200-nm change in plate's thickness at 1 mm, which approximately corresponds to a λ/4-change of the plate's thickness within the probe-beam diameter, the measured transmittance conforms to the transmittance of the incoherent light. This phenomenon can be seen by a comparison between the black and the red curves in Fig. 2 (d). The similarity with the results of the incoherent light is a consequence of measuring the transmittance of the whole beam, which gives an average transmittance of the distorted beam profile. However, the intensity at any particular point of the transmitted beam will show the interference oscillations.

When the plate is employed as a variable laser attenuator, the precise manipulation of the plate's transmittance is important. From the results presented in Fig. 2 it can be concluded that it is difficult to control the plate's transmittance with the incident angle. A more accurate manipulation can be achieved by changing the plate's thickness. This can be done most conveniently by heating the dielectric plate.

The change of a phase-shift difference for one round trip in the plate, δ, in a linear approximation depends on the plate's temperature change as:

#121165 - $15.00 USD Received 9 Dec 2009; revised 13 Jan 2010; accepted 28 Jan 2010; published 11 Feb 2010

$$\delta(\Delta T) \approx 2kn_0 d_0 \left(1 + \left(\underbrace{\alpha + \frac{\partial n}{\partial T}}_{\alpha_{d,n}} \right) \Delta T \right) \cos(\theta_t). \qquad (11)$$

Here, ΔT denotes the temperature change; n_0 and d_0 are initial refractive index and the plate's thickness, respectively; α is the linear temperature coefficient; and $\partial n / \partial T$ shows the change of the refractive index with the plate's temperature. We will combine the last two coefficients, α and $\partial n / \partial T$, in a linear coefficient $\alpha_{d,n}$.

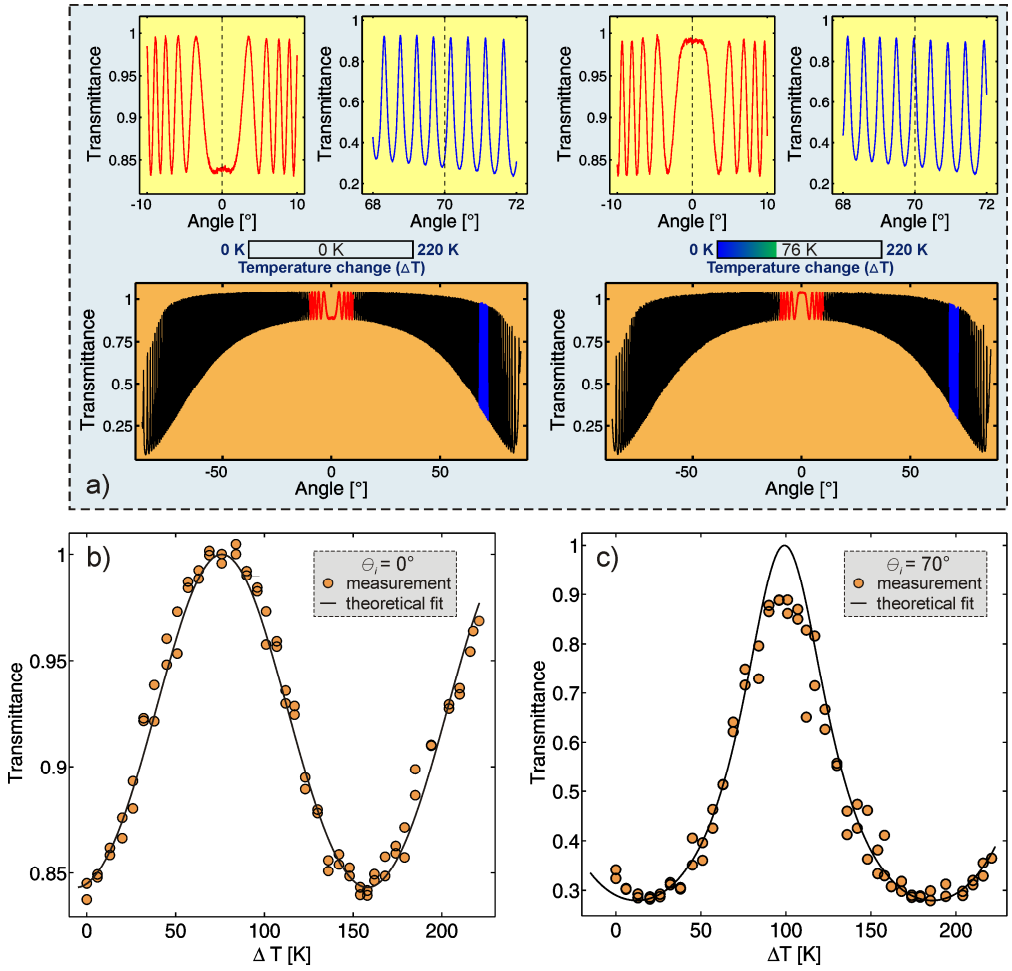

Fig. 3. a) The transmittance as a function of the incident angle at different plate temperatures (Media 1). b) Measured transmittance as a function of the temperature change for normal incidence of the probe beam. c) Measured transmittance as a function of temperature change at $\theta_i = 70°$. The black curve shows the theoretical fit.

The measured transmittance of the s-polarized light at all the incident angles as a function of the plate's temperature, shown in Fig. 3, demonstrates the utilization of a dielectric plate as a variable laser attenuator. The upper two graphs in Fig. 3(a) (Media 1) show the magnification of the transmittance for incident angles around θ_i = 0° and θ_i = 70°, respectively. It is clear that the temperature change of ΔT ~75 K alters the transmittance at normal incidence from its trough to its peak value. Therefore, at normal incidence, one fringe occurs during the ΔT ~150 K.

#121165 - $15.00 USD Received 9 Dec 2009; revised 13 Jan 2010; accepted 28 Jan 2010; published 11 Feb 2010

A quantitative evolution of the attenuator's transmittance as a function of the temperature change ΔT for particular angles $\theta_i = 0°$ and $\theta_i = 70°$ is shown as the circles in Figs. 3(b) and 3(c), respectively. The black curves show a theoretical fit according to Eq. (9), where the temperature-dependent phase-shift difference $\delta(\Delta T)$, defined by Eq. (11), was involved. The fitting parameters, d_0 and $\alpha_{d,n}$, obtained with the least-squares method, are equal to 140 μm ± 0.080 μm, and 10^{-5} K^{-1} ± 10^{-6} K^{-1}, respectively. For normal incidence (Fig. 3(b)) the transmittance trough value equals ~0.84, while the transmittance peak value reaches ~1. The transmittance changes periodically with a period of ΔT ~150 K. This period increases with the angle of incidence and is equal to 180 K at $\theta_i = 70°$ (Fig. 3(c)). Here, the measured transmittance is in the interval between 0.29 and 0.9. Therefore, the dielectric plate applied as an attenuator at this incident angle has a 4 times greater dynamic range than at normal incidence. This is a consequence of the higher reflectivity of the plate's surface according to Eq. (1). The difference in the peak values between the fitted (the black curve) and the measured transmittance appears at large angles because the limited beam and the wedge effects are not taken into account in Eq. (9).

When the absorption of the laser energy within the plate is significant, the temperature-dependent attenuation is considered as an unwanted effect. This phenomenon is visible in Fig. 4(a), showing the measurement of the plate's transmittance for the He-Ne probe beam during the absorption of the excitation-laser pulses. Figure 4(b), which is a magnification of the first 1.5 s of Fig. 4(a), reveals the rapid change of the plate's transmittance during each 50 ms. This period corresponds to the frequency of the excitation laser. The temperature change caused by an individual pulse can be estimated by a comparison of the results presented in Figs. 3(b) and 4(b). In this way we estimated that a single pulse increased the plate's temperature by ΔT ~4 K. This value is comparable with the temperature rise calculated by the specific heat equation, where the heat equals the absorbed pulse energy (12.5 mJ).

The temperature profile within the plate depends on the excitation-beam profile, the absorption coefficient and the thermal diffusivity. However, in our case the He-Ne probe beam was crossed concentrically with the larger excitation-laser beam. Therefore the transmittance within the probe-beam cross-section was approximately constant. We confirmed this by measurements of the transmittance for the probe beam, which was slightly moved out of the center of the excitation-laser beam.

The transmittance changes approximately sinusoidally with temperature, since the dielectric plate at normal incidence can be considered as a FPE with a low finesse. Therefore, the change of transmittance, caused by a single pulse, depends on the sub-fringe region. In the region where the FPE's response has a peak value, e.g., at $t = 0.4$ s in Fig. 4(b), the single pulse changes the transmittance by 1%. On the other hand, the transmittance does not change at the troughs and peaks, where the FPE's response is zero.

During the first few pulses of the excitation laser, the temperature of the plate is only slightly different to the environmental temperature. So, the heat losses due to conduction and radiation are small. As a consequence, the temperature of the plate between two successive pulses stays approximately constant, as can be seen from the time interval between 0 and 0.5 s in Fig. 4 (b). The heat dissipation increases with the plate's temperature. This leads to a considerable temperature drop between two pulses, as is visible from the time interval between 0.8 s and 1.5 s in Fig. 4(b). Steady-state conditions (the red curve in Fig. 4(c)) are achieved when the temperature losses during two pulses are equal to the temperature rise caused by a single pulse. In our case this happened at around the time $t = 10$ s, i.e., when the first 200 pulses were absorbed into the plate. The steady-state conditions depend on the excitation-laser power, absorption coefficient and the thermal properties of the plate.

When the laser was switched off, the plate started to cool, as can be seen from the blue curve in Figs. 4(a) and 4(c). Since the plate's heat is continuously dissipating during the cooling, there are no discrete "steps" in the transmittance change.

#121165 - $15.00 USD Received 9 Dec 2009; revised 13 Jan 2010; accepted 28 Jan 2010; published 11 Feb 2010

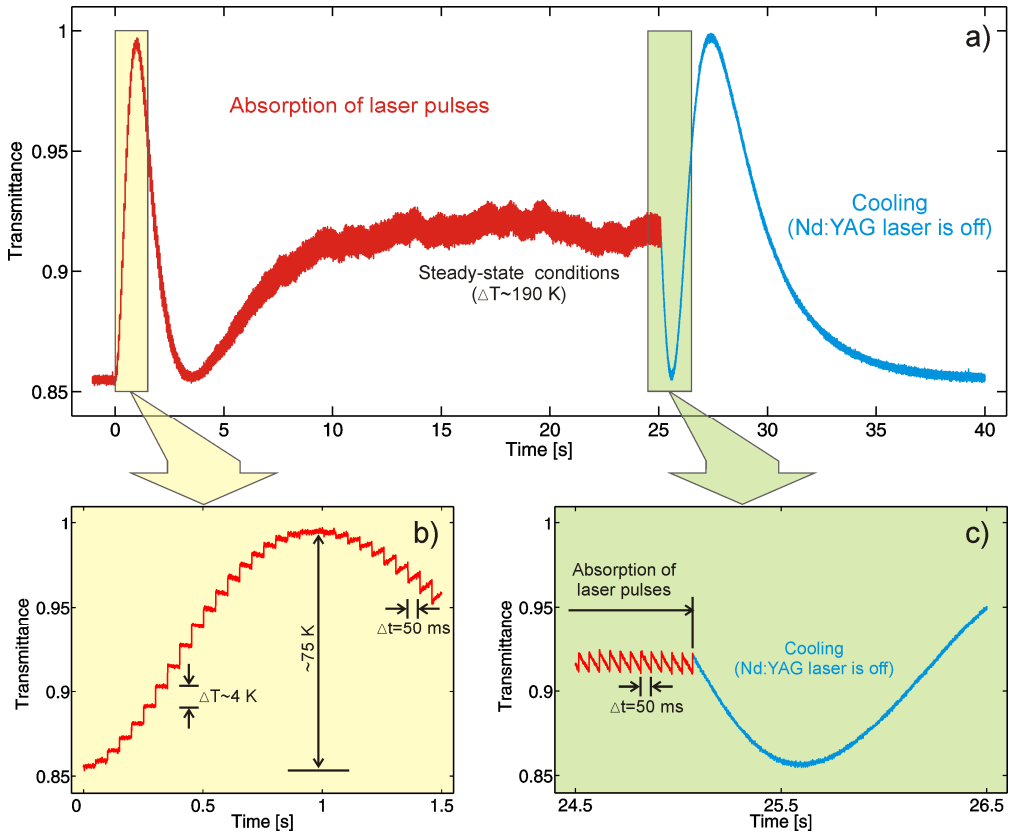

Fig. 4. The measurement of the plate's transmittance for the probe beam during the absorption of the excitation laser pulses. a) The entire measurement in the time period of 40 s. In the first 25 s a total of 500 pulses were absorbed in the plate, increasing its temperature from room temperature to 490 K. After that the excitation laser was switched off and the transmittance was measured during the plate's cooling. b) The magnification of the transmittance shows discontinuous changes of the transmittance for each laser pulse. c) When the temperature losses during two pulses equal the temperature rise caused by a single pulse, steady-state conditions are achieved (the red curve). The blue curve shows the plate's transmittance during spontaneous cooling.

In our study we measured the transmittance for the He-Ne probe beam with negligible absorption, while the excitation laser was used as a heating source. Therefore in this case the attenuation depends only on the temperature-dependent interference effects caused by the heating due to the absorption of the excitation-laser energy. On the other hand, when the excitation laser with a significant (but finite) absorption is attenuated its attenuation depends on the interference-effects as well as on the absorption within the plate. The first effect depends on the laser-pulse energy and the absorption coefficient of the dielectric plate, and varies with time until the steady-state conditions are achieved. The second effect depends on the absorption coefficient and the plate's thickness and stays approximately constant.

The described, unwanted temperature-dependent effects should be taken into account when a dielectric plate with a significant absorption is involved in high-power-laser applications. This is especially important when only a few pulses [17,18] are used. In this case steady-state conditions cannot be achieved and, therefore, the intensity of the beam transmitted through the plate varies with time.

5. Conclusion

We have presented theoretical and experimental results relating to the interference effects caused by Fresnel reflections on the boundaries of a dielectric plate. These results reveal the

#121165 - $15.00 USD Received 9 Dec 2009; revised 13 Jan 2010; accepted 28 Jan 2010; published 11 Feb 2010

typical behavior of multiple-reflected beams interfering with each other, which manifests itself in the plate's transmittance oscillations. We investigated their dependence on the incident angle of the laser beam, the plate's parallelism and the plate's temperature. These effects are interesting because of the wide range of laser applications where dielectric plates are involved as Brewster windows, etalons, or variable high-power attenuators.

The influences of small wedges, a limited (Gaussian) beam, and the polarization of the incident light were presented and explained in the case of angle-dependent interference effects. On the other hand, the plate's temperature changes its thickness and refractive index. We have demonstrated that this phenomenon can be used for a precise manipulation of the plate's transmittance. In such a way, a thin dielectric plate with temperature regulation can be used as a simple and robust variable attenuator for high-power-laser pulses. Here, the attenuation should be achieved by the interference, rather than the absorption within the plate. Therefore, an appropriate plate material should be selected, e.g., borosilicate glass for visible light and near IR, or sapphire for near and middle UV.

When the absorption of the laser energy within the plate is significant, unwanted temperature-dependent interference effects need to be taken into account. We have shown that the transmittance of the plate in this case changes in a step-like fashion with the frequency of the laser pulses. However, this effect can be neglected after a sufficient number of laser pulses, once steady-state conditions are achieved.

#121165 - $15.00 USD Received 9 Dec 2009; revised 13 Jan 2010; accepted 28 Jan 2010; published 11 Feb 2010